Frequency Limit for the Pressure Compliance Correction of Ocean-Bottom Seismic Data

Chao An*1, S. Shawn Wei², Chen Cai³, and Han Yue⁴

Abstract

Vertical records of ocean-bottom seismographs (OBSs) are usually noisy at low frequencies, and one important noise source is the varying ocean-bottom pressure that results from ocean-surface water waves. The relation between the ocean-bottom pressure and the vertical seafloor motion, called the compliance pressure transfer function (PTF), can be derived using background seismic data. During an earthquake, earthquake signals also generate ocean-bottom pressure fluctuations, and the relation between the oceanbottom pressure and the vertical seafloor motion is named the seismic PTF in this article. Conventionally, we use the whole pressure records and the compliance PTF to remove the compliance noise; the earthquake-induced pressure and the seismic PTF are ignored, which may distort the original signals. In this article, we analyze the data from 24 OBSs with water depth ranging from 107 to 4462 m. We find that for most stations, the investigated frequency range (0.01-0.2 Hz) can be divided into four bands depending on the water depth. In band (I) of lowest frequencies (<0.11, <0.05, and <0.02 Hz for water depth of 107, 1109, and 2650 m, respectively), the vertical seafloor acceleration is composed mostly of pressure compliance noise, which can be removed using the compliance PTF. The compliance PTF is much smaller than the seismic PTF, so distortion of earthquake signals is negligible. In band (II) of higher frequencies (0.11-0.20, 0.05-0.11, and 0.02-0.05 Hz for water depth of 107, 1109, and 2650 m, respectively), the vertical acceleration and ocean-bottom pressure are largely uncorrelated. In bands (III) and (IV) of even higher frequencies (> 0.11 and > 0.08 Hz for water depth of 1109 and 2650 m, respectively), the compliance noise is negligible, and the ocean-bottom pressure is mostly caused by the seafloor motion. Thus, the compliance can be safely ignored in frequency band (I).

Cite this article as An, C., S. Shawn Wei, C. Cai, and H. Yue (2020). Frequency Limit for the Pressure Compliance Correction of Ocean-Bottom Seismic Data, *Seismol. Res. Lett.* **91**, 967–976, doi: 10.1785/0220190259.

Supplemental Material

Introduction

It is known that the vertical recordings of ocean-bottom seismographs (OBSs) are contaminated at low frequencies, primarily due to two noise sources. One is the horizontal noise, possibly associated with ocean-bottom currents, leaking into the vertical channel when the instrument is not perfectly vertically leveled. The other is the seafloor compliance due to loading by oceansurface water waves (e.g., <0.04 Hz; Webb and Crawford, 1999). Long-period water waves penetrate the ocean water layer and cause vertical deformation of the seafloor. Such seafloor deformation can be utilized along with the ocean-bottom pressure to infer the underlying Earth structure (Yamamoto and Torii, 1986; Crawford et al., 1998; Zha et al., 2014). On the other hand, removal of such noise can greatly enhance the signal-tonoise ratio of the recorded earthquake signals. This now becomes a routine procedure widely applied to process longperiod earthquake signals, after which the earthquake signals can be utilized to investigate the Earth structure of areas of geological interests, such as the Eastern Lau Spreading Center (Wei *et al.*, 2015), the Cascadia subduction zone (Bell *et al.*, 2016; Bowden *et al.*, 2016; Tian and Ritzwoller, 2017; Janiszewski *et al.*, 2019), the central Pacific Ocean (Lin *et al.*, 2016; Agius *et al.*, 2017; Doran and Laske, 2019), and the Mariana subduction zone (Cai *et al.*, 2018).

Most OBSs are instrumented with a seismometer and a pressure gauge. A well-developed method to remove the noise

^{1.} Key Laboratory of Hydrodynamics (Ministry of Education), School of Naval Architecture, Ocean and Civil Engineering, Shanghai Jiao Tong University, Shanghai, China; 2. Department of Earth and Environmental Sciences, Michigan State University, East Lansing, Michigan, U.S.A.; 3. Guangdong Provincial Key Laboratory of Geodynamics and Geohazards, School of Earth Sciences and Engineering, Sun-Yat Sen University, Guangzhou, China; 4. School of Earth and Space Sciences, Peking University, Beijing, China

^{*}Corresponding author: anchao@sjtu.edu.cn

[©] Seismological Society of America

within the seismic records induced by ocean-surface water waves is to calculate and utilize a compliance pressure transfer function (PTF). A compliance PTF describes the relation between ocean-bottom pressure recorded by the pressure gauge and the vertical seafloor deformation recorded by the seismometer (Webb, 1998; Webb and Crawford, 1999, 2010; Crawford and Webb, 2000; Dolenc et al., 2007). It is derived using background seismic data without significant earthquake signals, so that the ocean-bottom pressure is predominately composed of surface water waves. In addition, earthquake signals cause ocean-bottom pressure fluctuations, which are recorded by the OBS pressure gauge as well. In this situation, the relation between the ocean-bottom pressure and the vertical seafloor motion is named the seismic PTF in this article. Thus, the pressure recordings actually consist of ocean-surface waves and earthquake-induced pressure changes. It is commonly assumed that the seismic PTF is much larger than the compliance PTF. As a result, one can use the whole pressure recordings and the compliance PTF to predict the seafloor deformation caused by the surface water wave, which is then subtracted from the records of vertical seafloor motion. However, using the whole pressure recordings may potentially distort the original earthquake signals in the vertical records (Bell et al., 2015).

To elaborate, the records of the vertical seafloor acceleration and ocean-bottom pressure during an earthquake, in the frequency domain, can be written as

$$\begin{cases} A(f) = A_w(f) + A_s(f) \\ P(f) = P_w(f) + P_s(f) \\ A_w(f) = T_w(f)P_w(f) & T_w : \text{compliance PTF} \\ A_s(f) = T_s(f)P_s(f) & T_s : \text{seismic PTF}, \end{cases}$$
(1)

in which A(f) is the Fourier transform of the vertical seafloor acceleration record, and it consists of the deformation due to ocean-surface waves, $A_w(f)$, and the earthquake signal, $A_s(f)$. P(f) is the Fourier transform of the ocean-bottom pressure record, and it also consists of the pressure due to ocean-surface waves, $P_w(f)$, and the earthquake signal, $P_s(f)$. The acceleration and pressure are connected by two different PTFs, the compliance PTF, $T_w(f)$, and the seismic PTF, $T_s(f)$. A(f), $A_w(f)$, $A_s(f)$, P(f), $P_s(f)$, $P_w(f)$, $T_w(f)$, and $T_s(f)$ are all complex functions. We emphasize that although $T_w(f)$ and $T_s(f)$ have the same units, they represent two different physical mechanisms. For $T_w(f)$, the ocean-bottom pressure change causes the vertical seafloor deformation; in contrast, for $T_s(f)$, the vertical seafloor motion causes the ocean-bottom pressure change. $T_w(f)$ can be obtained from in situ OBS records during quiet times when earthquake signals are absent; $T_s(f)$ has a theoretical solution depending on the water depth assuming incompressible water, as will be shown later in the article. From equation (1), by removing the pressure compliance noise A_w , we obtain

$$A_{s}(f) = A(f) - A_{w}(f) = A(f) - T_{w}P_{w}(f)$$

$$= A(f) - T_{w}(P(f) - P_{s}(f))$$

$$= A(f) - T_{w}P(f) + \frac{T_{w}}{T_{s}}A_{s}(f).$$
(2)

In reality, the total pressure P(f) instead of the water wave pressure $P_w(f)$ is used to remove the compliance noise. Equivalently, the last term of equation (2) is ignored. For this assumption, it is necessary that the last term of equation (2) should be negligible. In deep water, the compliance PTF T_w is supposed be much smaller than the seismic PTF T_s ($T_w \ll T_s$) (Crawford and Webb, 2000). This means that the earthquake signal A_s generates an ocean-bottom pressure A_s/T_s , and this pressure subsequently causes seafloor deformation T_wA_s/T_s , which is much smaller than the earthquake signal A_s itself. Therefore, equation (2) can be approximated to

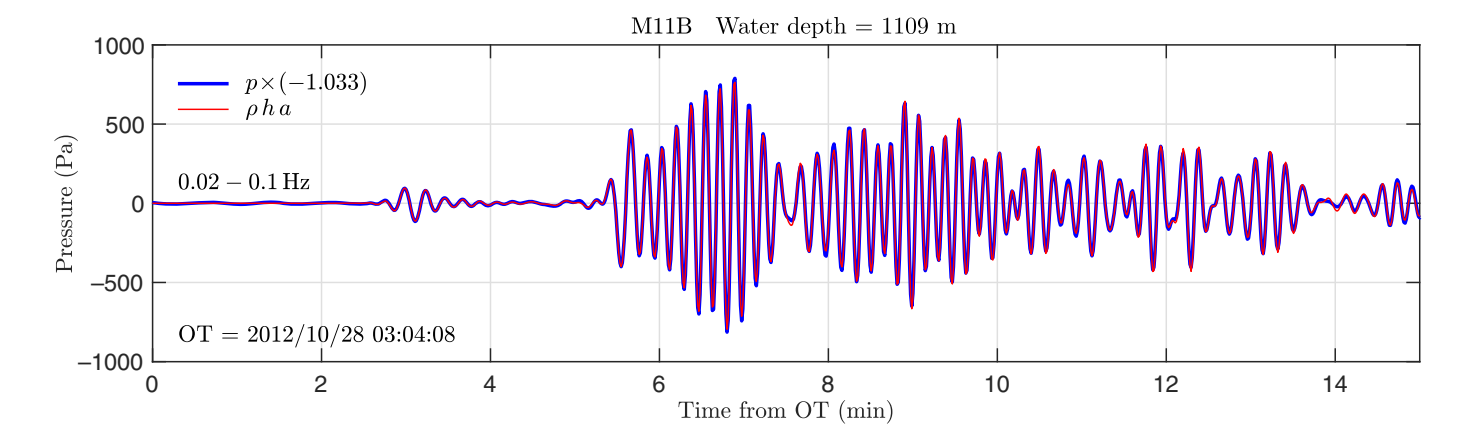
$$A_s(f) = A(f) - T_w P(f). \tag{3}$$

In shallow water, the pressure compliance noise becomes significant at high frequencies, so it is sometimes necessary to remove compliance noise at high frequencies. Because the amplitude of the compliance PTF is found to increase with frequency, it is inferred that it might reach the order of the seismic PTF at high frequencies, and thus neglecting the seismic PTF may cause distortion of the original earthquake signals (Bell et al., 2015). Ruan et al. (2014) and Bell et al. (2015) computed the seismic PTF from both earthquake events and noise, which was named the Rayleigh-wave transfer function in their papers because the OBS noise is mostly fundamental Rayleigh waves (Sutton and Barstow, 1990; Harmon et al., 2007; Yao et al., 2011). In this study, we will adopt a very simple theoretical solution of the seismic PTF and show its relation with the compliance PTF.

In this article, we analyze the data from 24 OBS stations of the Cascadia Initiative, with water depth ranging from 107 to 4462 m. The investigated frequency range is 0.01–0.2 Hz (5–100 s). We identify the frequency limit for the pressure compliance correction at each station. In addition, we develop a theoretical solution of the seismic PTF assuming incompressible water, and we find that it is much larger than the compliance PTF in the frequency range of interest. Therefore, equation (3) is shown to be a good approximation of equation (2). Thus, below the identified frequency, it is safe to ignore the seismic PTF and use equation (3) to remove the compliance noise.

Data Processing

The data are from 24 OBSs of the Cascadia Initiative (Toomey *et al.*, 2014). These stations are chosen because the water depth varies in a wide range, so that it is possible to analyze the relation between the vertical seafloor motion and ocean-bottom



pressure for different frequencies and water depth. All the instruments were provided by Scripps Institution of Oceanography, and each OBS consists of a three-component seismometer and a differential pressure gauge (DPG). DPGs measure the change of water pressure, and they are known to suffer from gain errors (Sheehan et al., 2015; Gusman et al., 2016; Zha and Webb, 2016; An et al., 2017; Doran and Laske, 2019). Basically, there exists a correction factor for each station, which can be multiplied by the pressure records to obtain the realistic ocean-bottom pressure. This is the reason that we chose the recording period of year 2012-2013 in this study. During the chosen investigated period, a relatively large earthquake (the 2012 $M_{\rm w}$ 7.8 Haida Gwaii earthquake) occurred, thus allowing an accurate correction of the pressure records. We first remove the instrumental response and convert the data to acceleration in m/s² and pressure in pascal for the vertical and pressure channels, respectively. A list of all the 24 stations and a map are given in Table S1 and Figure S1, available in the supplemental material to this article.

Pressure correction

The pressure sensors at all of the 24 OBS stations are DPGs, and the amplitude has to be calibrated to obtain the realistic ocean-bottom pressure. For each station, the correction factor can be obtained by matching the pressure records with predictions from the vertical seafloor acceleration. At relatively low frequencies, when water compressibility can be ignored, that is, the period of seafloor motion is much larger than the travel time of sound in the water from seafloor to sea surface, the pressure records p(t) and vertical seafloor acceleration a(t) during an earthquake are demonstrated to satisfy (An *et al.*, 2017)

$$cp(t) = \rho ha(t), \tag{4}$$

in which ρ is the water density, h is the water depth, c denotes the correction factor, and cp(t) gives the correct ocean-bottom pressure. In Figure 1, we show an example of correcting the pressure at station M11B. The data are from the 2012 $M_{\rm w}$ 7.8 Haida Gwaii earthquake and filtered between 0.02 and 0.1 Hz.

Figure 1. Pressure correction at station M11B. The records of the differential pressure gauge are multiplied by a constant -1.033 and plotted in blue. The theoretical ocean-bottom pressure calculated using equation ρha is plotted in red. The color version of this figure is available only in the electronic edition.

It is seen that after applying a correction factor of -1.033, the pressure perfectly matches the prediction from the seafloor acceleration. The pressure correction for all of the 24 stations is provided in Figure S2. The correction factors are summarized in Table S2. It is observed that the sign of the correction factor is largely associated with the type of pressure sensors. The sensors of ABALONES-4 \times 4 give negative correction factors, and the sensors of QEP - Q330 Environ and Quanterra Q330 Lin give positive correction factors.

Theoretical seismic PTF

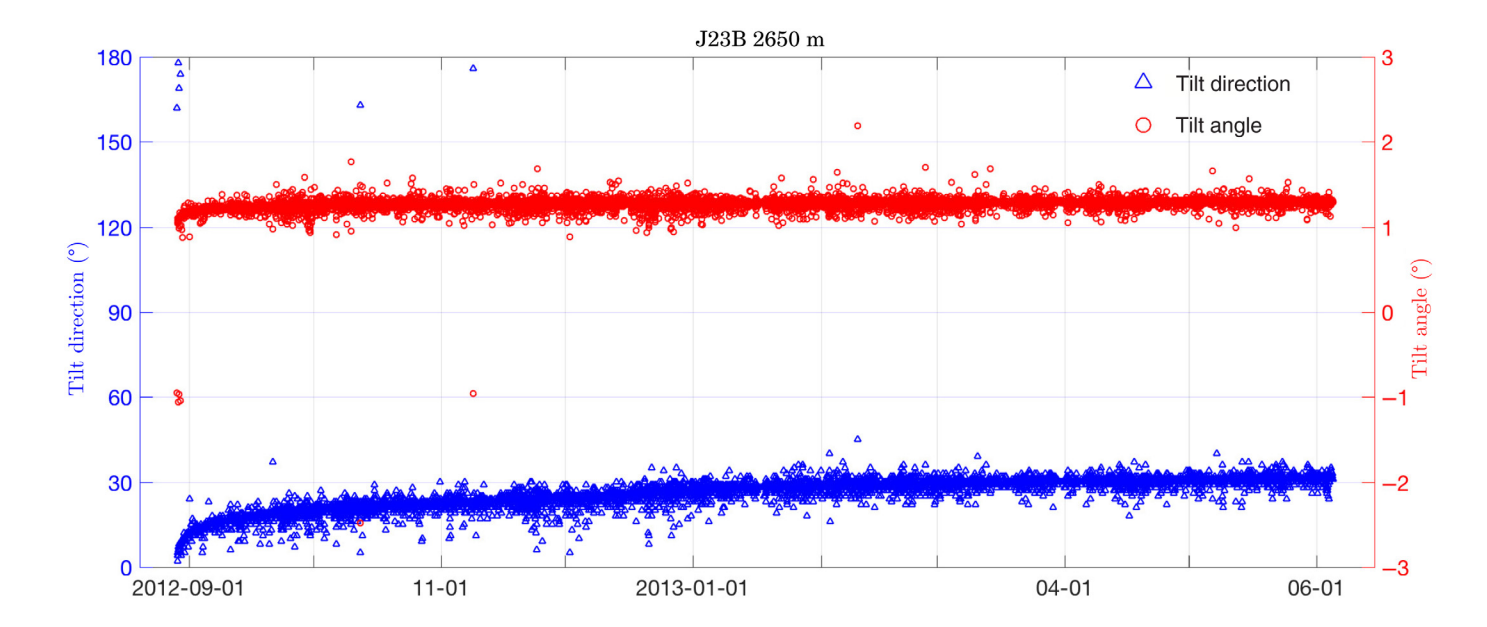
Because the vertical seafloor acceleration and ocean-bottom pressure satisfy equation (4) during an earthquake, the seismic PTF at a station can be readily obtained, which is a constant depending on the water depth, that is

$$T_s(f) = \frac{a(t)}{cp(t)} = \frac{1}{\rho h}.$$
 (5)

We note here that this equation is valid at relatively low frequencies when water compressibility is negligible. At high frequencies, the seismic PTF should be expressed by a modified equation to account for water compressibility, and the solution is not a constant but varies with frequency and the underlying Earth structure (Ruan *et al.*, 2014).

Instrument tilt noise

The goal of this article is to investigate the behavior of compliance noise in OBS data, so it is necessary to remove other noise in the vertical records before the analysis. Tilt noise is another major noise source for the recorded vertical seismograms, as mentioned in the Introduction. At some stations, the tilt noise dominates the vertical records over the compliance



noise, and so it is desirable to remove the tilt noise before we are able to analyze the compliance noise. We follow the procedure described by Bell et al. (2015) to calculate the instrument tilt parameters and remove the tilt noise. The continuous records are first filtered between 0.01 and 0.1 Hz and cut into small segments with time length of 1800 s. Narrower frequency ranges in 0.01-0.1 Hz and different time lengths up to 10,000 s have also been tested, and the results of instrument tilt are essentially the same. The two horizontal components of each data segment are rotated in the horizontal plane to find the maximum coherence between the first horizontal component and the vertical component. The rotation angle gives the tilt direction of the instrument with respect to the first horizontal direction. After rotating the horizontal components to the tilt direction, the tilt angle of the instrument with respect to the vertical direction can be derived from the coherence between the first horizontal component and the vertical component. An example of the tilt angles at station J23B is shown in Figure 2.

At some stations, the coherence between the horizontal channel and the vertical channel is very weak, indicating that the tilt noise is not dominant in the vertical component. This is possibly because the tilt angle is very small and thus the leaking of noise from the horizontal to vertical direction is negligible or because the ocean-bottom current is weak at this station so that it does not induce significant noise. For these stations where the tilt noise is insignificant, the tilt noise is not removed. The results of the instrument tilt at all of the 24 stations are given in Figure S3.

Computed PTFs

After removing the tilt noise in the vertical channel, we calculate the compliance PTF for each station. We filter the data in narrow frequency ranges with frequency intervals of about 0.02 Hz, that is, 0.01-0.02 Hz, 0.02-0.04 Hz, 0.04-0.06 Hz, ..., 0.18-0.2 Hz, and derive the compliance PTF for each

Figure 2. The instrument tilt at station J23B. The tilt direction provides the strike angle of the instrument in the horizontal plane with respect to the first direction of the ocean-bottom seismograph (OBS). The tilt angle gives the angle of the instrument with respect to the vertical direction. The color version of this figure is available only in the electronic edition.

frequency range. Using narrow frequency ranges, we are able to ensure high coherence between the vertical component and the pressure. The continuous records are cut into small segments of duration 10,000 s. We only use those segments with coherence greater than 0.8 between the vertical acceleration and the pressure. After the calculation of the compliance PTF for each frequency range, the results are combined to give the compliance PTF for the frequency range 0.01-0.2 Hz. Examples of the computed PTFs at three representative OBS stations are shown in Figure 3, where the water depths are 107, 1109, and 2650 m, respectively.

In Figure 3, we first observe that there is a sharp increase of the PTF. For example, the bottom panel of Figure 3 shows the computed PTF at station J23B, and it is found that the PTF increases dramatically at a frequency of about 0.02 Hz. The reason is explained as follows. Below 0.02 Hz, ocean-surface water waves have long wavelengths, and they can penetrate the water column and cause seafloor deformation. Thus, the vertical acceleration is dominated by the seafloor deformation due to ocean-bottom pressure, and the computed PTF is exactly the compliance PTF. It is also observed that, in this frequency range, the compliance PTF is much smaller than the theoretical seismic PTF. Above 0.02 Hz, ocean-surface water waves hardly penetrate the ocean water layer, and the coupling mechanism between the vertical seafloor acceleration and the ocean-bottom pressure is different. For the data segments, when the vertical and pressure channels are highly correlated, the vertical acceleration is dominated by microseisms,

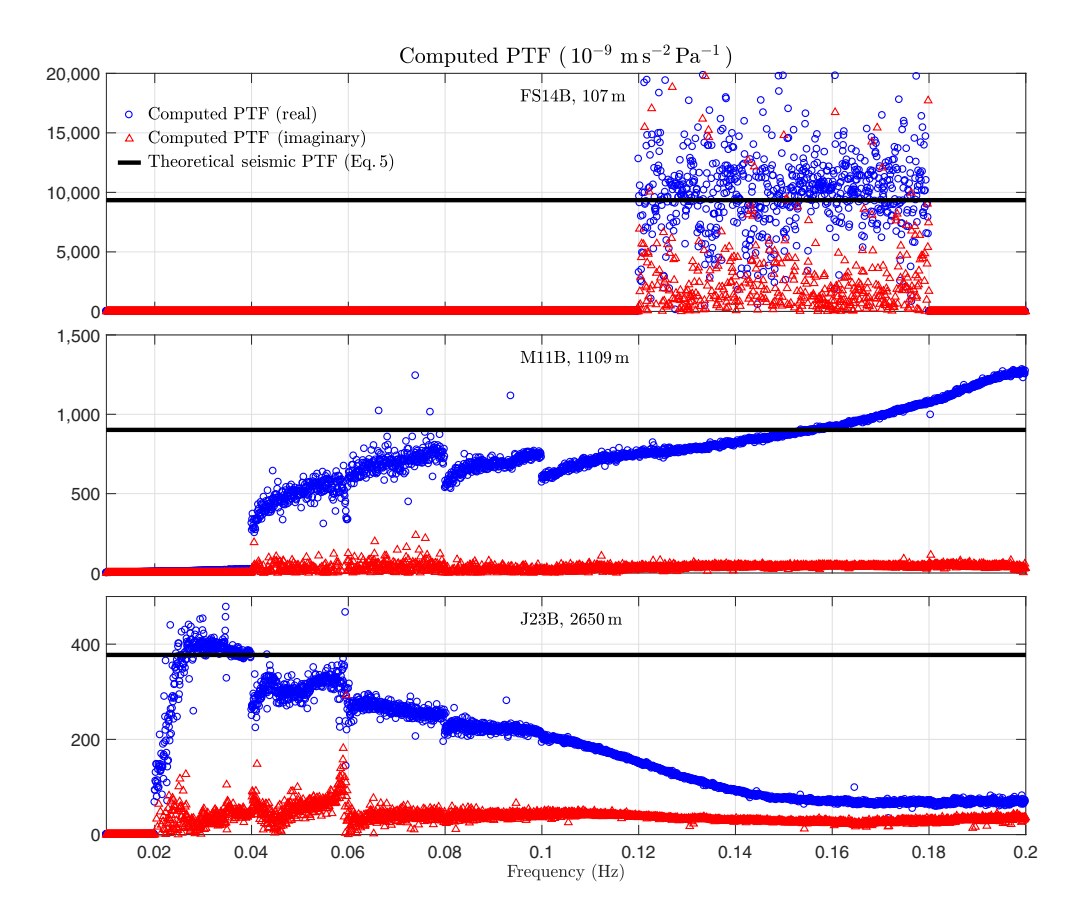


Figure 3. The computed and theoretical pressure transfer functions (PTFs) at three representative stations. The theoretical PTF is calculated using equation (5) assuming incompressible water. The color version of this figure is available only in the electronic edition.

and the pressure is generated from the seafloor motion accelerating the water column above the station. Thus, the computed PTF above 0.02 Hz shown in the bottom panel of Figure 3, which is found to be almost the same as the seismic PTF, is indeed the seismic PTF. At even higher frequencies, water compressibility is not negligible, and so the computed PTF deviates from our theoretical seismic PTF that ignores water compressibility.

From Figure 3, we also find that the real part of the PTF is much larger than the imaginary part. This indicates that both the elastic solid Earth and the water respond almost instantaneously to loading. For instance, at station J23B, below 0.02 Hz, the elastic solid Earth responds to the pressure loading almost instantaneously without phase lag; above 0.02 Hz, the water column also responds to the seafloor motion instantaneously. The PTF below 0.02 Hz is not clearly observable due to the plot scale, and it is shown with more details in Figure 4. The originally computed PTFs at all of the 24 stations are plotted in Figure S4.

Results

In Figure 4, we show the PTFs resulting at the same three representative OBS stations as shown in Figure 3. More results at

all of the 24 OBS stations are provided in Figure S5. In Figure 4, only the computed PTFs at relatively low frequencies are plotted, which are the real compliance PTFs. As mentioned in the previous section, the computed PTFs at high frequencies are actually the seismic PTFs, and they are not included in this figure.

It is observed that both the real and imaginary parts of the compliance PTF increase linearly with frequency. Thus, we can use a linear fit to infer the compliance PTF at higher frequencies. It is also found that the real part of the compliance PTF is much larger than the imaginary part, indicating an almost instantaneous response of the elastic Earth to the pressure loading. This can be explained by a simplified 2D half-space elastic model of uniform materials. Ignoring gravity, the governing equation of the solid Earth is written as

$$\rho \ddot{\mathbf{U}} = \nabla \cdot \mathbf{\sigma},\tag{6}$$

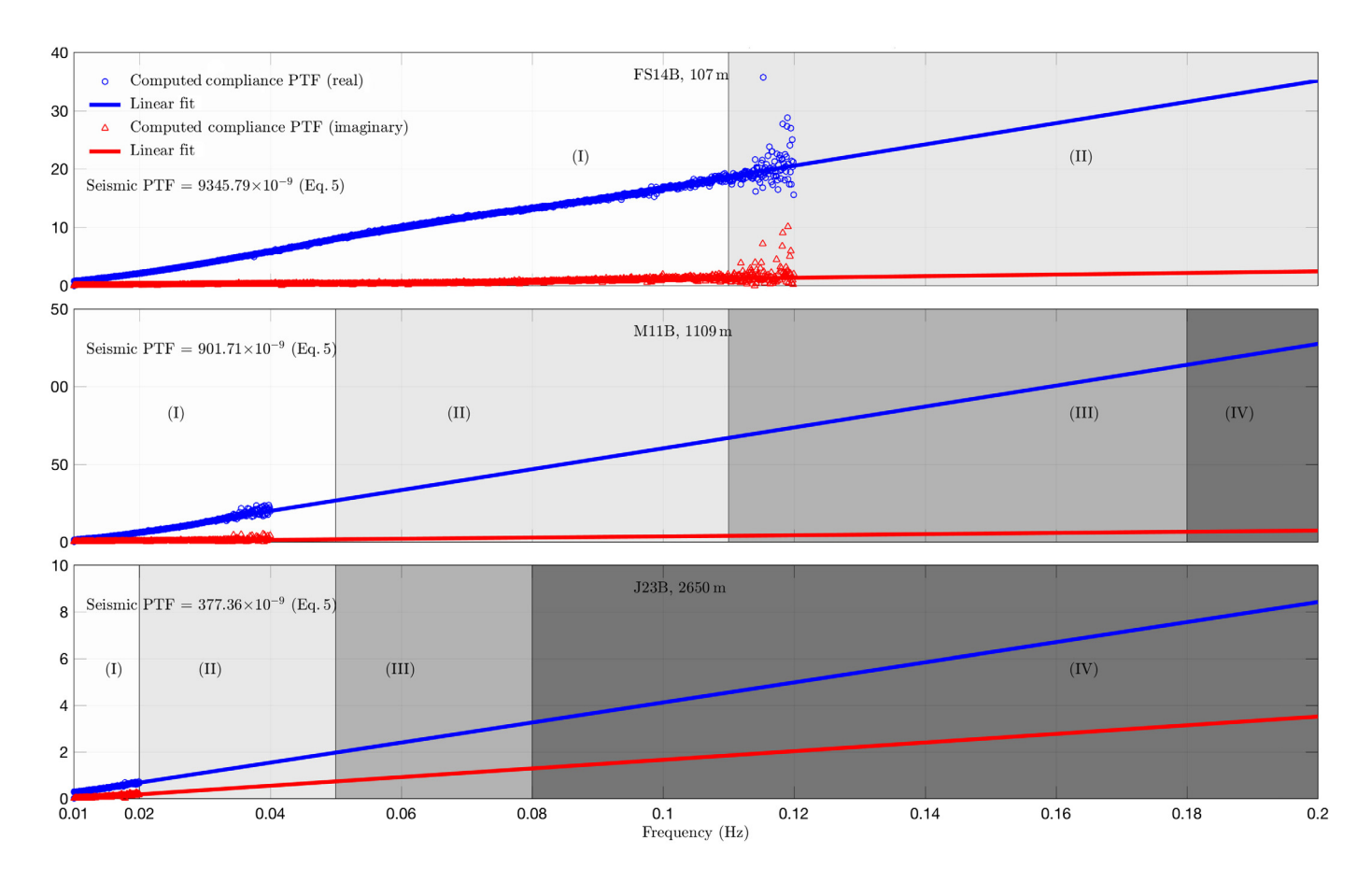
in which ρ is the density, $\mathbf{U}(x,z,t)$ is the displacement vector, (\cdot) represents dot product, and $\sigma(x,z,t)$ is the stress tensor. With z axis pointing upward from the seafloor, the boundary conditions are

$$\begin{cases} \sigma_{zz}(x, z, t)|_{z=0} = -P_0 e^{i(kx - \omega t)} \\ \sigma_{xz}(x, z, t)|_{z=0} = 0 \\ W(x, z, t)|_{z=-\infty} = 0, \end{cases}$$
 (7)

in which W(x, z, t) is the vertical displacement, and $P_0e^{i(kx-\omega t)}$ is the ocean-bottom pressure at z=0. The vertical acceleration is found to be (Crawford, 2004; An and Liu, 2016)

$$a(x, z, t)|_{z=0} = \frac{\sqrt{1 - \xi_{\alpha}} \xi_{\beta}}{4\sqrt{(1 - \xi_{\alpha})(1 - \xi_{\beta})} - (2 - \xi_{\beta})^2} \frac{\omega^2}{k\mu} P_0 e^{i(kx - \omega t)},$$
(8)

in which $\xi_{\alpha}=c^2/\alpha^2$, $\xi_{\beta}=c^2/\beta^2$, $c^2=\omega^2/k^2$, α , and β are the P- and S-wave velocities, respectively, and μ is the shear modulus of the Earth. Assuming that the ocean-surface water waves travel much more slowly than the seismic waves, that is, $c^2\ll\alpha^2$



and $c^2 \ll \beta^2$, equation (8) is expanded with respect to ξ_α and ξ_β near 0 to obtain

$$a(x,z,t)|_{z=0} \approx \frac{\alpha^2}{2(\alpha^2 - \beta^2)} \frac{\omega^2}{k\mu} P_0 e^{i(kx - \omega t)} = \frac{\lambda + 2\mu}{2\mu(\lambda + \mu)} \frac{\omega^2}{k} P_0 e^{i(kx - \omega t)},$$
(9)

in which λ is the Lamé first parameter. Assuming the oceansurface waves are long, we have $c^2 = \omega^2/k^2 \approx gh$, in which h is the water depth, leading to

$$a(x, z, t)|_{z=0} \approx \frac{\lambda + 2\mu}{2\mu(\lambda + \mu)} \omega \sqrt{gh} P_0 e^{i(kx - \omega t)}.$$
 (10)

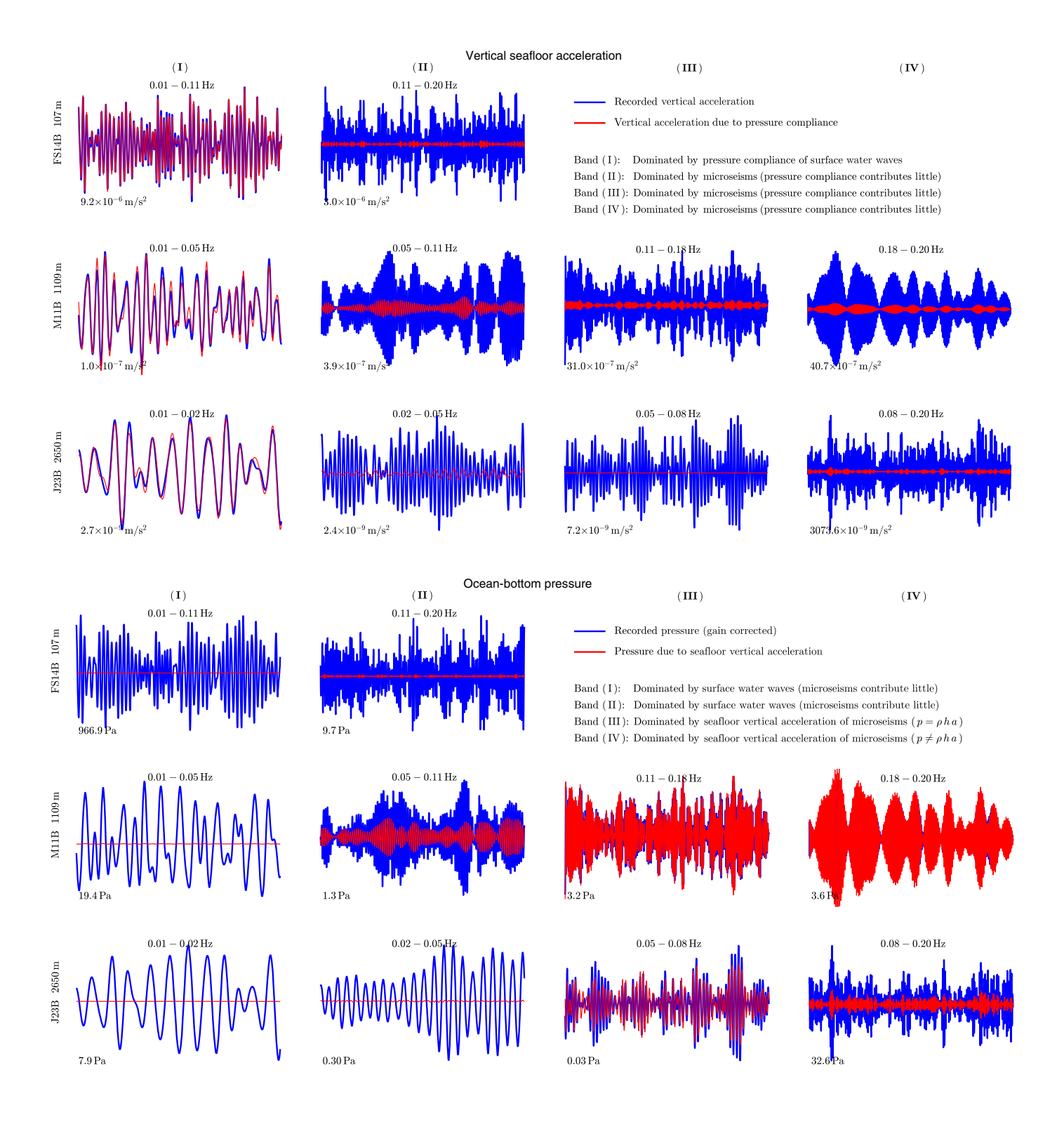
This analytical solution indicates that the compliance PTF is linearly proportional to frequency, which is consistent with our calculated results.

In addition, Figure 4 shows that the compliance PTF is much smaller than the theoretical seismic PTF given by equation (5). Although the compliance PTF increases with frequency, it is observed that the inferred compliance PTF at high frequencies is still much smaller than the theoretical seismic PTF. Therefore, it is safe to use equation (3) as an approximation of equation (2) to remove pressure compliance noise.

In Figure 4, four frequency bands are identified for each station and indicated by a different background color. Station FS14B only has two bands because of its shallow water

Figure 4. Computed compliance PTF and linear fit at three representative OBS stations. The seismic PTF is too large to be shown in the plot, and because it is a constant for relatively low frequencies, its value is given on the left of each panel. The color version of this figure is available only in the electronic edition.

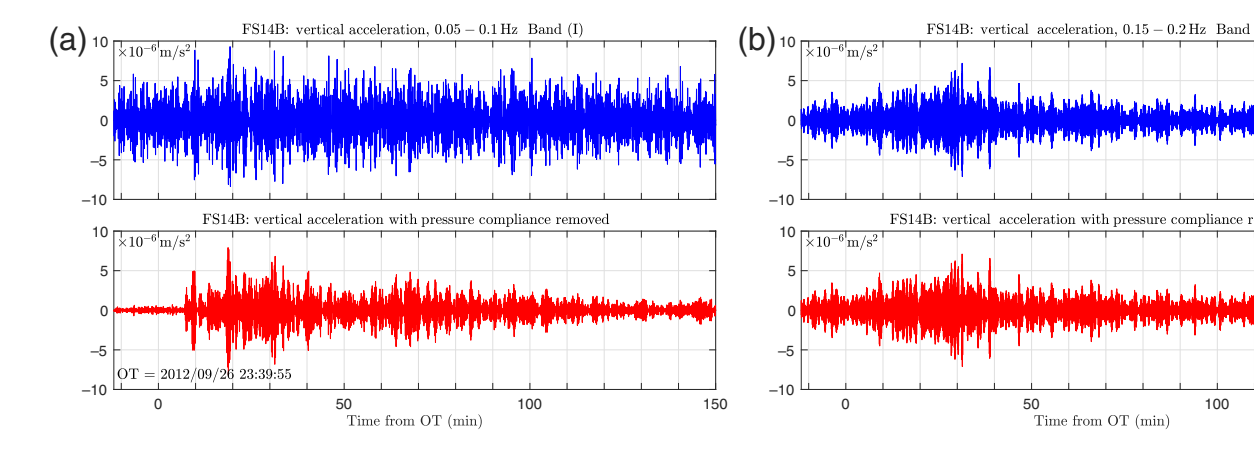
depth. For each station and frequency band, we compare the seismograms of the vertical seafloor acceleration and oceanbottom pressure to examine their relation. The duration of the seismograms is 3000 s, and the beginning time is 2012/ 10/10:00:00:00, both of which are chosen somewhat arbitrarily only to ensure that the seismograms are dominated by noise without significant earthquake signals. The seismograms are filtered in a series of frequency ranges of frequency intervals 0.01 Hz, that is, 0.01-0.02 Hz, 0.02-0.03 Hz, 0.03-0.04 Hz, ..., 0.19-0.20 Hz. Then, the records of the vertical seafloor acceleration, the predictions of the vertical seafloor acceleration from the pressure compliance using compliance PTF, the records of the ocean-bottom pressure, and the predictions of the ocean-bottom pressure from the seafloor acceleration using seismic PTF are calculated and compared. It is found that the investigated frequencies can be classified into four frequency bands, according to the relation between the vertical seafloor acceleration and ocean-bottom pressure. The seismograms at the three representative stations are plotted in Figure 5 for illustration. Because the four frequency bands



are determined using the selected 3000 s noise samples at each station, instead of averaging all the available recordings, the exact limits of the four frequency bands agree with, but do not exactly follow, the change of the computed PTFs.

In the upper three rows of Figure 5, the recorded vertical seafloor acceleration is filtered in the four frequency ranges and plotted in blue. The predicted seafloor acceleration from ocean-bottom pressure using the compliance PTF is plotted in red. The frequency limits of the four bands are different at the

Figure 5. Seismograms in the four frequency bands at the three representative stations. In the upper three rows, the recorded vertical seafloor acceleration is plotted in blue, and the seafloor acceleration predicted by pressure compliance is plotted in red. In the lower three rows, the recorded ocean-bottom pressure is plotted in blue, and the pressure predicted by seafloor acceleration is plotted in red. The value below each plot indicates the maximum recorded acceleration or pressure. The color version of this figure is available only in the electronic edition.



three OBS stations. Here for high frequencies where the calculated compliance PTFs are not available, we have also used the linear fit of the compliance PTF to do the predictions.

It is found that, in band (I), the predicted seafloor acceleration matches the records very well, indicating that the vertical seafloor acceleration is dominated by the pressure compliance in this frequency band. Therefore, it is feasible to remove the compliance noise from the vertical seismic records using the compliance PTF and enhance the signal-to-noise ratio. The upper limit of frequency band (I) generally depends on the water depth. In many of the previous studies, it is assumed that water waves of wavelength equal to or greater than the water depth can penetrate the water column, and consequently the upper limit of frequency band (I) can be calculated from the dispersion relation of ocean-surface water waves (Crawford et al., 1998; Bell et al., 2015). Our results show that the exact frequency limit can be higher than the estimate. For instance, at station M11B with water depth 1109 m, the upper frequency limit of band (I) is determined to be 0.05 Hz by manually checking the seismograms. It corresponds to water waves of wavelength 624 m, which is about 0.56 times the water depth. In other words, water waves of wavelength about half of the water depth generate compliance noise at station M11B. In bands (II)-(IV), the predictions of the vertical seafloor acceleration are negligible compared to the records or other noise, indicating that the noise in the seafloor acceleration is from different sources, and removal of the compliance noise will not improve the data quality.

In the lower three rows of Figure 5, the recorded ocean-bottom pressure is filtered in the four frequency ranges and is plotted in blue. The predicted pressure from the seafloor acceleration using the theoretical seismic PTF (equation 5) is plotted in red. It can be seen that in band (I) because the pressure records are dominated by ocean-surface waves, the predictions from the seafloor acceleration contribute very little. In band (II), the predictions from the seafloor acceleration are still insignificant. Band (II) differs from band (I) in that, in band (II), the pressure compliance also contributes little to the vertical seafloor acceleration, as shown in the upper three rows. Thus, the vertical seafloor acceleration and the ocean-bottom pressure are largely uncorrelated in band (II). In band (III), it is

Figure 6. The records of vertical seafloor acceleration before and after removal of compliance noise at station FS14B (water depth 107 m). (a) Frequency band (I); (b) frequency band (II). The color version of this figure is available only in the electronic edition.

150

found that the predicted pressure from seafloor acceleration matches the records very well. Therefore, the pressure in band (III) is generated mostly by the seafloor motion accelerating the water column. In band (IV), the pressure records and the predictions are found to have the same phase but different amplitudes. This is because the ocean-bottom pressure in band (IV) is still generated by seafloor motion, similar to band (III), but the theoretical seismic PTF by equation (5) must be corrected to account for water compressibility at high frequencies. Also, the correction factors for pressure records could possibly be different at high frequencies in band (IV) compared to low frequencies in band (III), which also harms the applicability of the theoretical seismic PTF in band (IV). More results at all of the 24 OBS stations are given in Figure S6.

From the earlier analysis, it is shown that compliance noise can be removed in frequency band (I), and the upper frequency limit of band (I) varies by station. The upper frequency limit of band (I) generally increases with water depth, and it can be higher than the traditional estimate that assumes wavelength equals water depth. Conventionally, compliance noise is removed at low frequencies for stations in deep water. If the water depth is shallow, compliance noise can be significant at high frequencies. Our analysis indicates that even at high frequencies the compliance PTF is still much smaller than the seismic PTF, and so the noise can also be removed similarly using the compliance PTF. Here, we show an example at a station where the water depth is very shallow (107 m), station FS14B. We select an $M_{\rm w}$ 6 earthquake, and the time and hypocenter of the earthquake are 26 September 2012 23:39:55 (UTC) and (51.592° N, 178.295° W, 16.0 km), respectively. The vertical seafloor acceleration at FS14B before and after the removal of the compliance noise, filtered in frequency band (I), are plotted in Figure 6a. Figure 6b shows the results in frequency band (II). It is clearly seen that, although the frequency in band (I) is higher than the traditional frequency for removal of compliance

noise (mostly <0.02 Hz), the removal of the compliance noise significantly improves the signal-to-noise ratio. Also, because the compliance PTF is much smaller than the seismic PTF, it is expected that the removal of the compliance noise causes little distortion of the earthquake signals. In band (II), although we can vaguely recognize the seismic signals at about 30 min, the removal of the compliance noise hardly improves the results, as the compliance noise is negligible compared to the overall noise level in this frequency range.

Conclusion

In this study, we analyze the data from 24 OBS stations with water depth of 107-4462 m and investigate the relation between the vertical seafloor acceleration and ocean-bottom pressure in different frequency ranges. The major findings are summarized as follows. For most stations, the investigated frequency range (0.01-0.2 Hz) can be divided into four bands. In band (I), the vertical seafloor acceleration is composed mostly of pressure compliance noise, and the noise can be removed by subtracting predictions from ocean-bottom pressure records. Both the real and imaginary parts of the compliance PTF increase linearly with frequency. The real part is much larger than the imaginary part, indicating almost instantaneous response of the elastic Earth to pressure loading. In addition, it is found that the compliance PTF is much smaller than the theoretical seismic PTF, even at high frequencies for stations in shallow water. Thus, using the total pressure that includes the earthquake signals to remove the pressure compliance noise causes little distortion of the earthquake signals. In band (II) of higher frequencies, the vertical seafloor acceleration and ocean-bottom pressure are largely uncorrelated, and thus the noise in the vertical acceleration cannot be removed using the pressure records. In bands (III) and (IV) of even higher frequencies, noise in the vertical acceleration is mostly microseisms, and the compliance noise is negligible. The ocean-bottom pressure is generated mostly by the vertical seafloor acceleration in bands (III) and (IV). The exact limits for each frequency band vary station by station and largely depend on the water depth. Particularly, the upper frequency limit of band (I) increases as water depth decreases, and it can be higher than the estimate from the water wave dispersion relation assuming that the wavelength of water waves is equal to the water depth.

Data and Resources

The ocean-bottom seismograph (OBS) data can be obtained from the Incorporated Research Institutions for Seismology (IRIS) Data Management Center at www.iris.edu (last accessed June 2019). More results for all of the 24 OBS stations are provided in the supplemental material.

Acknowledgments

This work made use of the Seismic Analysis Code (SAC) and Generic Mapping Tools (GMT) software. The authors thank Associate Editor

John Ebel for many editorial corrections on this article. This work is supported by the National Nature Science Foundation of China Grant 11632012 and U1901602 (C. An), the 2018 Shanghai Pujiang Program (C. An), and National Science Foundation Grant OCE-1842989 (S. S. Wei).

References

- Agius, M. R., C. A. Rychert, N. Harmon, and G. Laske (2017). Mapping the mantle transition zone beneath Hawaii from *Ps* receiver functions: Evidence for a hot plume and cold mantle downwellings, *Earth Planet. Sci. Lett.* **474**, 226–236.
- An, C., and P. L. Liu (2016). Analytical solutions for estimating tsunami propagation speeds, *Coast. Eng.* **117**, 44–56.
- An, C., C. Cai, Y. Zheng, L. Meng, and P. Liu (2017). Theoretical solution and applications of ocean bottom pressure induced by seismic seafloor motion, *Geophys. Res. Lett.* **44**, no. 20, 10,272–10,281.
- Bell, S., Y. Ruan, and D. W. Forsyth (2016). Ridge asymmetry and deep aqueous alteration at the trench observed from Rayleigh wave tomography of the Juan de Fuca plate, *J. Geophys. Res.* **121**, no. 10, 7298–7321.
- Bell, S. W., D. W. Forsyth, and Y. Ruan (2015). Removing noise from the vertical component records of ocean-bottom seismometers: Results from year one of the Cascadia Initiative, *Bull. Seismol. Soc. Am.* **105**, no. 1, 300–313.
- Bowden, D., M. D. Kohler, V. Tsai, and D. S. Weeraratne (2016). Offshore Southern California lithospheric velocity structure from noise crosscorrelation functions, *J. Geophys. Res.* 121, no. 5, 3415–3427.
- Cai, C., D. A. Wiens, W. Shen, and M. Eimer (2018). Water input into the Mariana subduction zone estimated from ocean-bottom seismic data, *Nature* **563**, no. 7731, 389.
- Crawford, W. C. (2004). The sensitivity of seafloor compliance measurements to sub-basalt sediments, *Geophys. J. Int.* **157**, no. 3, 1130–1145.
- Crawford, W. C., and S. C. Webb (2000). Identifying and removing tilt noise from low-frequency (<0.1 Hz) seafloor vertical seismic data, *Bull. Seismol. Soc. Am.* **90**, no. 4, 952–963.
- Crawford, W. C., S. C. Webb, and J. A. Hildebrand (1998). Estimating shear velocities in the oceanic crust from compliance measurements by two-dimensional finite difference modeling, *J. Geophys. Res.* **103**, no. B5, 9895–9916.
- Dolenc, D., B. Romanowicz, R. Uhrhammer, P. McGill, D. Neuhauser, and D. Stakes (2007). Identifying and removing noise from the Monterey ocean bottom broadband seismic station (MOBB) data, *Geochem. Geophys. Geosys.* 8, no. 2, doi: 10.1029/2006GC001403.
- Doran, A., and G. Laske (2019). Seismic structure of marine sediments and upper oceanic crust surrounding Hawaii, *J. Geophys. Res.* **124**, no. 2, 2038–2056.
- Gusman, A. R., A. F. Sheehan, K. Satake, M. Heidarzadeh, I. E. Mulia, and T. Maeda (2016). Tsunami data assimilation of Cascadia seafloor pressure gauge records from the 2012 Haida Gwaii earthquake, *Geophys. Res. Lett.* **43**, no. 9, 4189–4196.
- Harmon, N., D. Forsyth, and S. Webb (2007). Using ambient seismic noise to determine short-period phase velocities and shallow shear velocities in young oceanic lithosphere, *Bull. Seismol. Soc. Am.* 97, no. 6, 2009–2023.
- Janiszewski, H. A., J. B. Gaherty, G. A. Abers, H. Gao, and Z. C. Eilon (2019). Amphibious surface-wave phase-velocity measurements of

- the Cascadia subduction zone, *Geophys. J. Int.* 217, no. 3, 1929–1948.
- Lin, P.-Y. P., J. B. Gaherty, G. Jin, J. A. Collins, D. Lizarralde, R. L. Evans, and G. Hirth (2016). High-resolution seismic constraints on flow dynamics in the oceanic asthenosphere, *Nature* 535, no. 7613, 538.
- Ruan, Y., D. W. Forsyth, and S. W. Bell (2014). Marine sediment shear velocity structure from the ratio of displacement to pressure of Rayleigh waves at seafloor, *J. Geophys. Res.* 119, no. 8, 6357–6371.
- Sheehan, A. F., A. R. Gusman, M. Heidarzadeh, and K. Satake (2015).
 Array observations of the 2012 Haida Gwaii tsunami using Cascadia Initiative absolute and differential seafloor pressure gauges, Seismol. Res. Lett. 86, no. 5, 1278–1286.
- Sutton, G. H., and N. Barstow (1990). Ocean-bottom ultralow-frequency (ULF) seismo-acoustic ambient noise: 0.002 to 0.4 Hz, *J. Acoust. Soc. Am.* **87**, no. 5, 2005–2012.
- Tian, Y., and M. H. Ritzwoller (2017). Improving ambient noise cross-correlations in the noisy ocean bottom environment of the Juan de Fuca plate, *Geophys. J. Int.* 210, no. 3, 1787–1805.
- Toomey, D. R., R. M. Allen, A. H. Barclay, S. W. Bell, P. D. Bromirski, R. L. Carlson, X. Chen, J. A. Collins, R. P. Dziak, B. Evers, et al. (2014). The Cascadia Initiative: A sea change in seismological studies of subduction zones, *Oceanography* 27, no. 2, 138–150.
- Webb, S. C. (1998). Broadband seismology and noise under the ocean, *Rev. Geophys.* **36**, no. 1, 105–142.

- Webb, S. C., and W. C. Crawford (1999). Long-period seafloor seismology and deformation under ocean waves, *Bull. Seismol. Soc. Am.* 89, no. 6, 1535–1542.
- Webb, S. C., and W. C. Crawford (2010). Shallow-water broadband OBS seismology, Bull. Seismol. Soc. Am. 100, no. 4, 1770–1778.
- Wei, S. S., D. A. Wiens, Y. Zha, T. Plank, S. C. Webb, D. K. Blackman, R. A. Dunn, and J. A. Conder (2015). Seismic evidence of effects of water on melt transport in the Lau back-arc mantle, *Nature* 518, no. 7539, 395.
- Yamamoto, T., and T. Torii (1986). Seabed shear modulus profile inversion using surface gravity (water) wave-induced bottom motion, *Geophys. J. Int.* 85, no. 2, 413–431.
- Yao, H., P. Gouedard, J. A. Collins, J. J. McGuire, and R. D. van der Hilst (2011). Structure of young East Pacific Rise lithosphere from ambient noise correlation analysis of fundamental- and higher-mode Scholte-Rayleigh waves, *Compt. Rendus Geosci.* 343, nos. 8/9, 571–583.
- Zha, Y., and S. C. Webb (2016). Crustal shear velocity structure in the Southern Lau basin constrained by seafloor compliance, *J. Geophys. Res.* **121,** no. 5, 3220–3237.
- Zha, Y., S. C. Webb, S. Nooner, and W. C. Crawford (2014). Spatial distribution and temporal evolution of crustal melt distribution beneath the East Pacific Rise at 9°–10° N inferred from 3-D seafloor compliance modeling, *J. Geophys. Res.* **119**, no. 6, 4517–4537.

Manuscript received 18 September 2019 Published online 5 February 2020